

Biosensing Performance of a Plasmonic-Grating-Based Nanolaser

Haoran Zhang^{1, ‡}, Jiacheng Sun^{2, ‡}, Jie Yang^{1, ‡},
Israel De Leon³, Remo Proietti Zaccaria^{4, *}, Haoliang Qian⁵,
Hongsheng Chen⁵, Gaofeng Wang^{1, *,} and Tao Wang^{1, *}

(Invited Paper)

Abstract—We introduce and numerically investigate a high-quality resonant structure formed by a dielectric low-order diffraction grating combining materials with high refractive index contrast. The proposed structure is capable of supporting multiple plasmonic modes owing to hybridization effects, modes having the characteristic of exhibiting remarkable sensing response to the change of the environment refractive index yet limited figure of merit. To improve the figure of merit, the proposed architecture is modified by adding a layer of semiconductor gain medium, as it can compensate the internal losses. The result is an active sensor showing multi-modal lasing behaviour, with very low threshold and large mode spacing. It is found that the device shows switchable response upon modification of the pump amplitude or polarization, a very important feature when it comes to sensing devices. Finally, the achieved figure of merit is 3400 RIU^{-1} , one order of magnitude higher than the passive case and much higher than the theoretical limit for sensors based on Kretschmann configuration. Thus, the proposed architecture possesses great potentials as an optical sensor for bio-detection and environmental monitoring.

1. INTRODUCTION

Over the past several decades, considerable efforts have been devoted to engineer electronic and photonic band structures for controlling the emission properties of optical devices [1, 2]. Nanophotonic structures with controllable coupling between photonic and electronic resonances are particularly interesting since they provide an impressive ability in tailoring light-matter interaction. In this respect, they have been exploited to explore intriguing phenomena such as optical resonances [3], electromagnetic induced transparency [4], plasmonic hybridization [5], and lasing [6, 7] together with fascinating applications such as optical storage devices [8, 9], photocatalytic processes [10, 11], high performance photovoltaics [12], on-chip lasers [13, 14], and optical sensors [15–19].

In particular, plasmonic-based optical sensors can benefit from the use of nanophotonic structures for a wide range of applications with improved performance. Indeed, either under the form of localized surface plasmon resonance (LSPR) [20] or surface plasmon polariton (SPP) [21], plasmonic-based sensors have the peculiarity to address operations at the nanoscale (subwavelength dimensions) featured by remarkable enhancement of the local electric field, leading to an extremely high sensitivity to the variations of the surrounding dielectric environment. Therefore, plasmonic-based optical sensors have been widely used in various real-time and label-free sensing applications [22].

Received 24 September 2021, Accepted 24 November 2021, Scheduled 29 October 2021

* Corresponding authors: Remo Proietti Zaccaria (remo.proietti@iit.it); Gaofeng Wang (gaofeng@hdu.edu.cn); Tao Wang (wangtao@hdu.edu.cn). ‡ The authors contribute equally to this work.

¹ School of Electronics and Information, Hangzhou Dianzi University, Hangzhou 310018, China. ² Key Laboratory of 3D Micro/Nano Fabrication and Characterization of Zhejiang Province, School of Engineering, Westlake University, 18 Shilongshan Road, Hangzhou 310024, Zhejiang Province, China. ³ School of Engineering and Sciences, Tecnológico de Monterrey, Monterrey, Nuevo León 64849, Mexico. ⁴ Italian Institute of Technology, via Morego 30, Genova 16163, Italy. ⁵ Interdisciplinary Center for Quantum Information, College of Information Science and Electronic Engineering, Zhejiang University, Hangzhou 310027, China.

Numerous sensor architectures relying on plasmonic-based mechanisms have been proposed [23, 24]. Among different sensing schemes, a well-developed method for SPPs generation is based on prism-induced total internal reflection, and it is applied in Kretschmann and Otto configurations [13, 25]. Although this approach exhibits significantly improved sensing performance, it also suffers from the disadvantage of requiring bulky sizes. Furthermore, the need of metallic materials for the generations of plasmonic-modes carries the inherent issue of ohmic losses in turn resulting in broad spectrum line widths. This issue becomes especially important at the subwavelength range, as it jeopardizes the further improvement of sensitivity and resolution.

In this work, we design and numerically study an active plasmonic grating structure consisting of a semiconductor gain medium sandwiched between a thin silver film and a high-contrast grating (HCG). Indeed, by combining the dielectric/metal interface to the low diffraction orders originating from the HCG, SPPs can be generated. The four-level gain medium is added in between the metal and HCG with the aim of realizing a pronounced hybrid-lasing behaviour with ultra-low threshold and extremely narrow linewidth. In particular, switchable lasing is observed by modifying either the pump intensity or the polarization. Finally, the compact laser device displays versatile sensing function through multiple responses associated with different generated modes, with an ultra-high sensing figure of merit (FOM) reaching values up to 3400 RIU^{-1} . This FOM, besides being much higher than the corresponding value for the passive case (i.e., gain medium free), represents also a remarkable improvement with respect to the state-of-art of active plasmonic sensors with a FOM around 1000 RIU^{-1} [6, 26]. Thus, the proposed device shows multi-mode switchable lasing operation and remarkable sensing performance, hence indicating great potential in applications such as high performance sensors also in liquid environments and multiband optical communication device.

2. STRUCTURE DESIGN AND MODE ANALYSIS

Figure 1 shows the geometrical and materials arrangement of the structure, with the materials refractive indexes chosen for $\lambda = 1.55 \mu\text{m}$. The structure starts with a SiO_2 bottom substrate ($n = 1.46$) followed by a 200 nm silver layer (Ag, $n = 0.16 + i11.35$). Then, when no lasing is considered (passive case), 100 nm InGaAsP-like buffer layer ($n = 3.3$) is added on top of the silver, as it can enhance the occurring resonances and control the generation of SPPs. Afterwards, a one-dimensional (1D) silicon nitride (Si_3N_4 , $n = 2.0$) rectangle-shape grating defined by periodicity P , width W and thickness T is arranged on the top of the buffer layer to modulate the permittivity of metal/dielectric interface for SPPs generation. The detailed material parameters are described in Table 1, and the values of refractive index for the given materials are obtained from [27–30]. For the practical fabrication, the deposition of different layers can be implemented by the advanced thin film processing technologies, such as magnetron sputtering, metal organic chemical vapor deposition (MOCVD), and pulsed laser deposition (PLD) methods. In the step of Si_3N_4 grating processing, a 500 nm layer of stoichiometric silicon nitride can be firstly grown by low-pressure chemical vapor deposition. Then, it can be patterned through using the electron beam lithography (EBL) method.

In order to demonstrate the biosensing function, we consider that the entire structure is immersed

Table 1. Geometrical and material parameters of the proposed device.

Material	Dimension and shape	Refractive index ($\lambda = 1550 \text{ nm}$)
H_2O	∞ (analyte)	1.33
Si_3N_4	$P_{\text{grating}} = 1160 \text{ nm}$	2.0
	$W_{\text{strip}} = 464 \text{ nm}$	
	$T_{\text{grating}} = 500 \text{ nm}$	
InGaAsP	$T_{\text{InGaAsP}} = 100 \text{ nm}$	3.3
Ag	$T_{\text{Ag}} = 200 \text{ nm}$	$0.16 + i11.35$
SiO_2	∞ (substrate)	1.45

in water ($n = 1.33$) in order to mimic a biological environment and illuminated by a TM-polarized ($E // x$ -axis) broad-spectrum light source traveling downward along the z -axis. To rule out the effect of finite size, we assume translational periodicity along x direction with Si_3N_4 stripes being infinitely long in y direction. Finally, the whole structure is simulated by Finite-Difference Time-Domain (FDTD) method, and the sensing performance of the device is numerically analyzed. The detailed simulation method is shown in S1 section of supplementary material.

Excited with normally incident radiation, the structure responds forming a photonic and a plasmonic modes, the former generated by the dielectric grating and the latter due to the presence of a dielectric/metallic interface. Meanwhile, the introduction of Ag layer plays a significant role in the generation of photonic and plasmonic modes. When there is no Ag layer, these two modes disappear (see Fig. 1 in supplementary material). In addition, further investigation indicates that these two modes undergo strong coupling condition [31] as clearly demonstrated in Fig. 1(b). In particular, the interaction of the two modes is verified by mapping the reflectance upon sweeping the grating period P , resulting in a clear anticrossing behaviour characterized by a Rabi splitting of the order of 5 meV [32–34]. The strong coupling behaviour is further confirmed by observing the electric field profiles which show two different situations, a mode confined in the metallic layer (left dashed line) and a grating localized mode (right dashed line). Apart from TM-polarized ($E // x$ -axis) pump, we also modified the pump polarization from TM- to TE-mode and studied the influence on the mode properties. As shown in Fig. 2 in supplementary material, we note that the tuning of pump polarization not only introduces an weakening of the two modes, but also excites another mode at $1.664 \mu\text{m}$ when the pump polarization angle is 30° , and it becomes more obvious with the pump polarization angle.

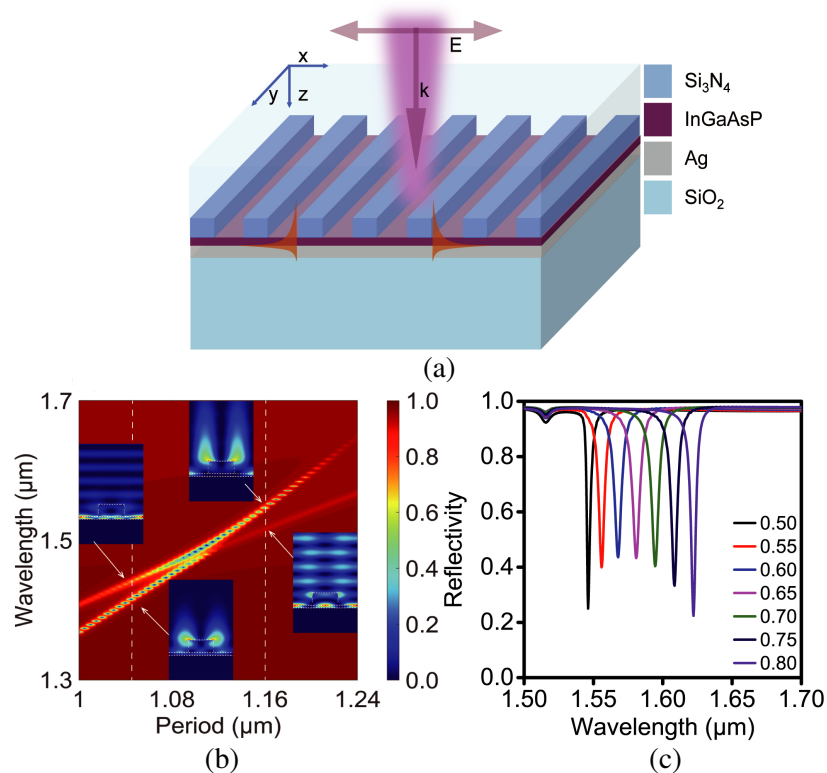


Figure 1. (a) Structure diagram of the hybrid plasmonic-grating sensor. (b) Reflectance map under different periods from $1 \mu\text{m}$ to $1.24 \mu\text{m}$. The insets show the electric field distributions of the photonic and plasmonic modes generated in the structure at the crossing points between the two vertical white dashed lines (period equal to $1.04 \mu\text{m}$ and $1.16 \mu\text{m}$) and the reflectance maxima. (c) Reflectance spectra under different Si_3N_4 grating thickness for $P = 1.16 \mu\text{m}$ and $W = 0.464 \mu\text{m}$.

To further analyze the hybrid behavior originating from dielectric/metal interface coupling to the photonic grating, the following equation based on wavevector matching condition can be employed [35]:

$$k_0 n_{en} \sin \theta + m \frac{2\pi}{P} = \pm k_0 \sqrt{\frac{\text{Re}(\varepsilon_{Ag}) \varepsilon_{eff}}{\text{Re}(\varepsilon_{Ag}) + \varepsilon_{eff}}} \quad (1)$$

where k_0 is the wave vector in vacuum; n_{en} is the refractive index of the ambient medium (water in the present case); θ is the angle of incidence with respect to the z -axis; m is the diffraction order; ε_{Ag} is the complex permittivity of silver; and ε_{eff} is the permittivity of an effective medium here comprising 100 nm of InGaAsP, Si₃N₄ stripes, and the environment material (i.e., all the materials on top of the metallic layer). For normally incident illumination, Eq. (1) leads to:

$$\lambda_m = \frac{P}{m} \sqrt{\frac{\text{Re}(\varepsilon_{Ag}) \varepsilon_{eff}}{\text{Re}(\varepsilon_{Ag}) + \varepsilon_{eff}}} \quad (2)$$

With these considerations in mind, we investigate the reflectance properties of the structure as the thicknesses of the Si₃N₄ grating elements is varied, namely the value of ε_{eff} . Fig. 1(c) shows the calculated reflectance for various grating-element thicknesses ranging from 0.5 to 0.8 μm . These results show two distinct modes, associated with the first and second order Bragg resonances of the grating. Interestingly, the first-order mode ($m = 1$), which occurs at wavelengths between 1.55 μm and 1.63 μm , is much more sensitive to the variation of the grating thickness than the second-order mode ($m = 2$) located at around 1.52 μm . A clear red-shift is indeed observed only for the $m = 1$ mode as the thickness of the grating elements increases. This behaviour can be understood through Eq. (2), and the value of ε_{eff} can be calculated through this formula, then $n_{eff} = \sqrt{\mu \varepsilon_{eff}}$ (where μ is the permeability of Si₃N₄, and $\mu \approx 1$ for nonmagnetic material). Indeed, upon an increase of T from 0.5 to 0.8 μm , the $m = 1$ mode correspondingly shows a large variation of n_{eff} from 1.2 to 1.4, while the value of n_{eff} for $m = 2$ mode keeps constant at 1.8.

The different properties of the two aforementioned modes are also reflected by their different bulk sensing performances. From Fig. 2(a) it can be seen that by altering the liquid environment refractive index the two modes exhibit different responses according to the peak position shifting. With a refractive index change of 5×10^{-4} RIU (Refractive Index Unit), the peak shifting of $m = 2$ mode is only ~ 0.08 nm, while $m = 1$ mode returns a wavelength variation as large as ~ 0.5 nm. Furthermore, both the modes show a linear dependence on the environment refractive index, as depicted in Fig. 2(b), a behaviour in good agreement with previous investigations [38, 39]. In terms of bulk sensitivity S_B , namely the peak shift per RIU defined as $\Delta\lambda/\Delta n$, where Δn is the change of bulk environment index, the value achieved by $m = 2$ mode is only 160 nm/RIU, while the sensitivity of $m = 1$ mode is about 1000 nm/RIU. This remarkable value is nearly four times larger than the recently reported advanced GMR sensor [36], a result suggesting a great potential for high performance sensing applications.

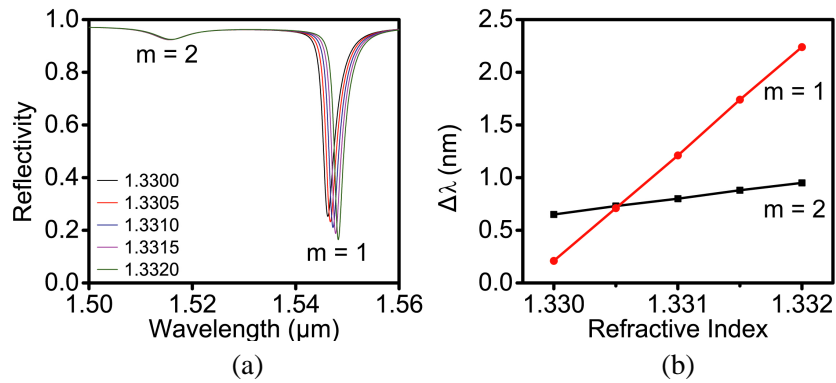


Figure 2. (a) Reflectance spectra of $m = 1$ and $m = 2$ modes with different environment refractive indexes. (b) Linear resonance peak shift of $m = 1$ mode (red line) and $m = 2$ mode (black line) as the function of environment refractive index.

However, due to the non-negligible loss of metal, even after the optimization of the structural parameters, the calculated full width at half maximum (FWHM) of the $m = 1$ mode results in several nanometers, and even tens of nanometers in other reports [37, 38], which significantly suppresses the figure of merit $FOM = S_B/\text{FWHM}$ of the sensor. In particular, in the present case the $m = 1$ and $m = 2$ modes show FOM as low as $\sim 363 \text{ RIU}^{-1}$ and $\sim 19 \text{ RIU}^{-1}$, respectively. Therefore, for improving the sensing performance of the proposed device, we develop one kind of active sensors through the employment of gain material to overcome the cavity losses and provide sharp lasing peaks with high sensing figure of merit.

3. LASING REALIZATION AND MODE DYNAMICS

Polarization-tunable multimodal plasmonic lasing has been recently reported based on gold nanoparticle superlattices [1]. Nevertheless, the introduced design requires complex fabrication process and possesses limited tunability. Here, we propose a hybrid plasmonic-grating laser through the replacement of the dielectric buffer layer with InGaAsP gain medium, achieving low threshold lasing and large tuning range over 100 nm around 1550 nm wavelength. The achieved results suggest that the proposed high performance IR tunable laser could be indeed meaningful to the nanoscale development of optical communication devices besides providing a good solution for ameliorating the limited FOM due to the aforementioned metallic loss.

To properly understand the mechanisms underneath the lasing behaviour of the hybridized structure, we have integrated a four-level one-electron system of semiconductor gain medium into our FDTD model [40]. In this respect, the geometrical parameters allowing for a proper overlap between the strongest mode (i.e., $m = 1$ mode) and the gain spectrum of InGaAsP at $1.55 \mu\text{m}$ are given by $P = 1.16 \mu\text{m}$, $T = 0.5 \mu\text{m}$, and $W = 4.64 \mu\text{m}$ (as mentioned, the $m = 2$ mode is located at $1.52 \mu\text{m}$ regardless the grating thickness variation, see Fig. 1(c)). Under the excitation of a TM polarized pump at $1.064 \mu\text{m}$, a pronounced lasing for $m = 1$ and $m = 2$ modes can be observed from the input-output light curves shown in Fig. 3. In particular, it is found that the $m = 1$ mode has a lower threshold (red line, $\sim 2.35 \times 10^6 \text{ V/m}$) than that of $m = 2$ mode (black line). In this regard, the laser intensity profiles shown in Fig. 3(a) can be understood by stressing two specific aspects related to the $m = 1$ mode: i) this mode has much narrower linewidth 2.8 nm leading to a Q factor much higher than that for the $m = 2$ mode ($Q_{m=1} \sim 560$, $Q_{m=2} \sim 164$) or, in different words, for the $m = 1$ mode case, the gain medium has to compensate a limited number of optical loss channels, surely a lower number than that for the $m = 2$ case; ii) The position of $m = 1$ mode is much closer to the center wavelength of the gain spectrum ($1.55 \mu\text{m}$), hence more gain can be exploited for lasing [1]. Another interesting behaviour emerging from Fig. 3(a) is that with the increase of the pump amplitude, the $m = 1$ output rapidly decreases after the rise of $m = 2$ mode. In detail, this behaviour is illustrated in Fig. 3(b), clearly showing a modes competition manifesting at pump amplitude equal to $2.8 \times 10^6 \text{ V/m}$. This mode competition behaviour could be attributed to the significantly different field distributions of the two modes, with the $m = 2$ mode confining more of its electric field inside the gain material than the $m = 1$ mode. Hence, the $m = 2$ mode can achieve a larger confinement factor f , which is the fractional overlap of electric field profile inside the gain medium to the whole plasmonic mode profile over the spatial dimension. The f factor can be calculated through the following formula [41, 42]:

$$f = \frac{\int_{\text{gain}} |\mathbf{E}^2(x, z)| dx dz}{\int_{-\infty}^{+\infty} |\mathbf{E}^2(x, z)| dx dz} \quad (3)$$

where $\int_{\text{gain}} |\mathbf{E}^2(x, z)| dx dy$ represents the integral of electric field intensity of the plasmonic mode in the InGaAsP layer, and $\int_{-\infty}^{+\infty} |\mathbf{E}^2(x, z)| dx dz$ indicates the total integral of electric field intensity over the (x, z) cross section of the hybrid plasmonic grating. After calculating the f factors by using the field distributions of the two modes (see Fig. 3(c)), it was found that the $m = 1$ mode possesses a much smaller confinement factor $f = 0.04$ than the $m = 2$ with a value equal to 0.25. Such a large

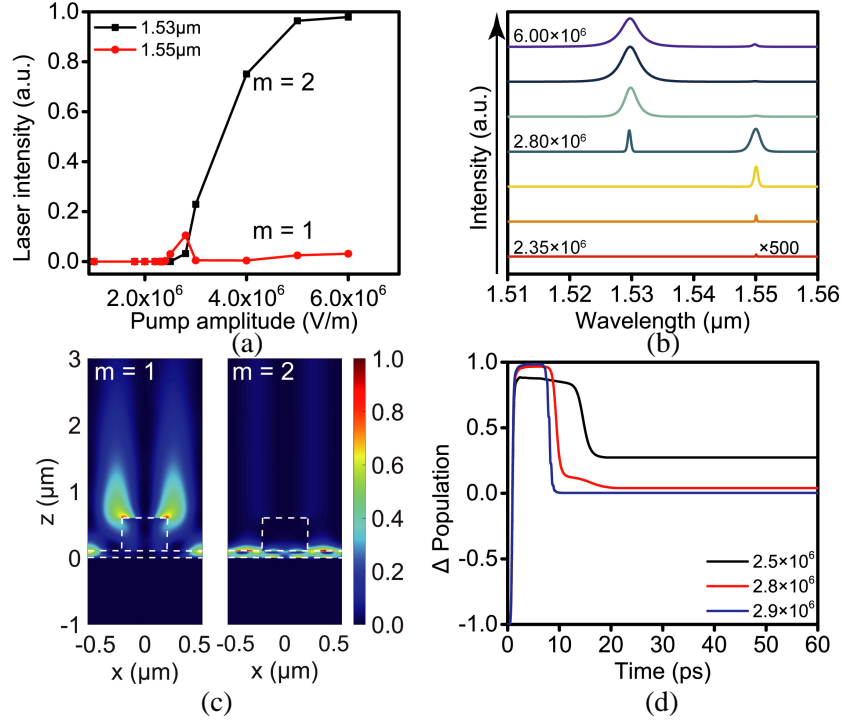


Figure 3. (a) Input-output light curve of $m = 1$ lasing mode (red line) threshold at 2.35×10^6 V/m and $m = 2$ lasing mode (black line) with threshold at 2.75×10^6 V/m. (b) Lasing spectra under different pump amplitudes, indicating mode competition behavior. (c) Mode profile of $m = 1$ mode (left) and $m = 2$ mode (right). (d) Population inversion as the function of time under different pump amplitudes.

difference facilitates the predominance of the $m = 2$ mode so that with larger pump fluence more energy is harvested by $m = 2$ mode, in turn inducing a stronger stimulated emission.

The mode competition behavior can also be analyzed through the variation of the population inversion. Fig. 3(d) displays the temporal evolution of inverted population for different pump levels. The curves show a decrease of the inverted population lifetime upon increase of the pump amplitude, since the stimulated emission induced a shortened lifetime for the inverted populations [43]. Interestingly, a small slope appears when the pump amplitude reaches 2.8×10^6 V/m (red curve in Fig. 3(d)), which suggests the simultaneous coexistence of $m = 1$ and $m = 2$ modes.

To further explore the dependence of mode dynamics on the pump source, the polarization of pump was gradually tuned from TM ($E // x$ -axis) to TE ($E // y$ -axis), as depicted in Fig. 4(a). Under TM pump excitation and for the same pump amplitude, e.g., 2.80×10^6 V/m, we observe the coexistence of $m = 1$ and $m = 2$ at $1.53 \mu\text{m}$ and $1.55 \mu\text{m}$, respectively. However, when the pump polarization is turned to 60° from TM, both the modes are replaced by a new mode at $1.674 \mu\text{m}$. This polarization dependence phenomenon can be explained as follows: (i) One-dimensional gratings are polarization-selective, hence the TE/TM modes can be excited separately under different pump polarizations; (ii) The semiconductor gain medium has a wide gain spectrum, which provides enough tolerance for a proper overlapping with both TE and TM modes [40]. Fig. 4(b) shows the lasing behaviour for the $1.674 \mu\text{m}$ mode, indicating a very low threshold at 1.85×10^6 V/m, much lower than that for $m = 1$ and $m = 2$ modes. The inset is the typical field distribution of lasing mode obtained at the same pump amplitude, and the hot spots between grating strips indicate that the low order diffraction modes possess much stronger intensity. Therefore, when the pump is horizontally polarized ($E // x$ -axis), the output lasing peaks are primarily of TM characteristics. In contrast, when the pump is vertically polarized ($E // y$ -axis), the lasing mode shows TE mode features. All these findings demonstrate that pump polarization is indeed a tool for controlling the switching between multi-mode and single-mode lasing, which might be promising for applications in optical sensing.

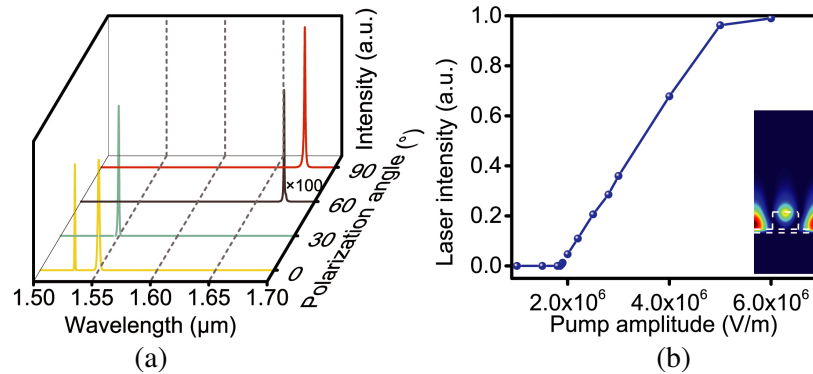


Figure 4. (a) Lasing peaks under different pump polarization (TM/ 0° , 30° , 60° and TE/ 90°). The $m = 1$ and $m = 2$ lasing modes can be seen at 0° . (b) Input and output light curve of TE lasing mode excited by TE pump polarization; inset, typical field distribution profile obtained at 2.80×10^6 V/m.

4. ACTIVE SENSING AND PERFORMANCE

Finally, to validate the proposed laser design as a refractometric sensor, the spectrum responses from different modes were investigated, and the results are shown in Fig. 5. All the considered modes display distinct red-shifting for a change in the environment refractive index equal to 5×10^{-4} , as depicted in Fig. 5(a), an important result as this polarization independent response can be exploited for multifunctional operations in biological applications when water, glucose, and even urea [44] are considered as environment materials. In terms of sensitivity, the results show that for $m = 2$ mode S_B is only 150 nm/RIU, while for $m = 1$ mode it reaches 850 nm/RIU. The distinct sensitivity difference is due to the field profile properties of two modes: $m = 1$ mode is on the top of gratings and shows much stronger localized field; however, $m = 2$ mode is localized within the buffer and Ag layers, resulting in a weaker interaction between light and matter. Interestingly, for the active case the sensitivity results are smaller than that for the passive case. However, due to the narrow spectral linewidth (only 0.25 nm), the FOM value for the $m = 1$ mode is equal to 3400 RIU^{-1} , almost one order magnitude higher than for the passive case. This is an remarkable finding as in the field of optical sensors FOM offers more comprehensive information on the evaluation of the sensing performance [45].

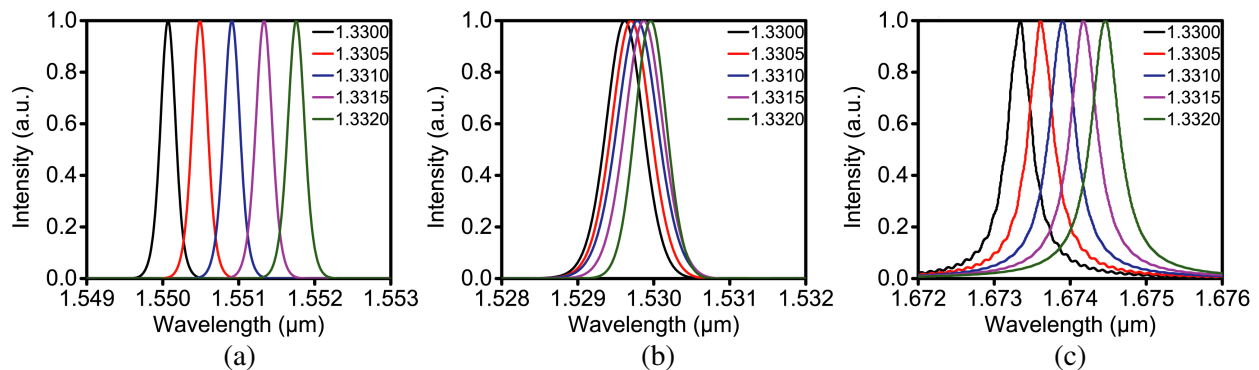


Figure 5. (a), (b) and (c) are lasing peaks of $m = 1$, $m = 2$ TM and TE lasing modes at $1.550 \mu\text{m}$, $1.530 \mu\text{m}$ and $1.674 \mu\text{m}$, respectively, with different environment RI from 1.3300 to 1.3320.

Table 2 summarizes the sensing performance of different modes obtained by controlling the pump polarization. We note that different modes possess different linewidths and different sensitivities, thus resulting in different figure of merits. Although there has been a number of reports on sensors based on plasmonic structures [46], hybrid resonators [47], and even based on active laser devices [48], this

Table 2. Comparison of sensing performance of different modes when lasing occurs.

Mode	Wavelength (μm)	FWHM (nm)	Sensitivity (nm/RIU)	FOM (RIU^{-1})
$\text{TM}_{(m=1)}$	1.550	0.25	850	3400
$\text{TM}_{(m=2)}$	1.529	0.56	150	600
TE	1.674	0.38	580	1526

is the first time that polarization was exploited as a tool for developing high-performance (i.e., high FOM) sensors. Furthermore, all the reported FOMs, regardless the considered mode, are much higher than the theoretically predicted upper FOM limit for sensors based on Kretschmann configuration [49] making the present approach very attractive.

5. CONCLUSIONS

In summary, we have designed and numerically studied a plasmonic device supporting plasmonic modes through the use of dielectric subwavelength HCGs. The device exhibits sensing functionality in liquid environment as it can identify refractive index change with high sensitivity, yet limited FOM. In order to improve the sensing figure of merit, we have then modified the proposed architecture in a way to compensate the internal losses by adding a layer of active material, demonstrated by a clear pump-dependent lasing behaviour. Furthermore, and most importantly, a strong pump polarization dependence of the lasing mode was observed, hence representing a very valuable method for tuning the lasing wavelength within a 140 nm range. Finally, we tested the sensing performance by checking the S_B and FOM values, with the results suggesting multiple responses from different modes, a very different situation from conventional plasmonic sensors. In fact, modes generated under different polarization pumps display higher FOM values than the passive device (lasing-free). In particular, we have achieved an ultra-high FOM value of 3400 RIU^{-1} at $1.55 \mu\text{m}$. These findings strongly suggest that the proposed innovative laser device may represent a feasible platform to achieve ultra-high performance refractive index sensing, a platform that can be readily applied also to biological environments.

ACKNOWLEDGMENT

This work is partially supported by several sources: the National Natural Science Foundation of China (Grant No. 61804036), Zhejiang Province Commonweal Project (Grant No. LGJ20A040001), National Key R & D Program Grant (Grant No. 2018YFE0120000), Zhejiang Provincial Key Research & Development Project Grant (Grant No. 2019C04003).

CONFLICT OF INTEREST

The authors declare no conflict of interest.

REFERENCES

1. Wang, D., A. Yang, W. Wang, Y. Hua, R. D. Schaller, G. C. Schatz, and T. W. Odom, "Band-edge engineering for controlled multi-modal nanolasing in plasmonic superlattices," *Nat. Nanotechnol.*, Vol. 12, 889–894, 2017.
2. Wang, K., H. Qian, Z. Liu, and P. K. L. Yu, "Second-order nonlinear susceptibility enhancement in gallium nitride nanowires (Invited)," *Progress In Electromagnetics Research*, Vol. 168, 25–30, 2020.
3. Miroshnichenko, A. E., S. Flach, and Y. S. Kivshar, "Fano resonances in nanoscale structures," *Rev. Mod. Phys.*, Vol. 82, 2257–2298, 2010.
4. Lezec, H. J., A. Degiron, E. Devaux, R. A. Linke, L. Martin-Moreno, F. J. Garcia-Vidal, and T. W. Ebbesen, "Beaming light from a subwavelength aperture," *Science*, Vol. 297, 820–822, 2002.

5. Prodan, E., C. Radloff, N. J. Halas, and P. Nordlander, "A hybridization model for the plasmon response of complex nanostructures," *Science*, Vol. 302, 419–422, 2003.
6. Sun, J. C., T. Wang, Z. Jafari, and I. De Leon, "High-Q plasmonic crystal laser for ultra-sensitive biomolecule detection," *IEEE J. Sel. Topics Quantum Electron.*, Vol. 27, 4601407, 2021.
7. Tao, T., T. Zhi, B. Liu, J. Dai, Z. Zhuang, Z. Xie, P. Chen, F. Ren, D. Chen, Y. Zheng, and R. Zhang, "Manipulable and hybridized, ultralow-threshold lasing in a plasmonic laser using elliptical InGaN/GaN nanorods," *Adv. Func. Mater.*, Vol. 27, 1703198, 2017.
8. Losurdo, M., Y. Gutiérrez, A. Suvorova, M. M. Giangregorio, S. Rubanov, A. S. Brown, and F. Moreno, "Gallium plasmonic nanoantennas unveiling multiple kinetics of hydrogen sensing, storage, and spillover," *Adv. Mater.*, Vol. 33, 2100500, 2021.
9. Song, M., D. Wang, Z. A. Kudyshev, Y. Xuan, Z. Wang, A. Boltasseva, V. M. Shalaev, and A. V. Kildishev, "Enabling optical steganography, data storage, and encryption with plasmonic colors," *Laser Photonics Rev.*, Vol. 15, 2000343, 2021.
10. Creel, E. B., E. R. Corson, J. Eichhorn, R. Kostecky, J. J. Urban, and B. D. McCloskey, "Directing selectivity of electrochemical carbon dioxide reduction using plasmonics," *ACS Energy Letters*, Vol. 4, 1098–1105, 2019.
11. Christopher, P., H. L. Xin, and S. Linic, "Visible-light-enhanced catalytic oxidation reactions on plasmonic silver nanostructures," *Nat. Chem.*, Vol. 3, 467–472, 2011.
12. Raja, W., A. Bozzola, P. Zilio, E. Miele, S. Panaro, H. Wang, A. Toma, A. Alabastri, F. De Angelis, and R. Proietti Zaccaria, "Broadband absorption enhancement in plasmonic nanoshells-based ultrathin microcrystalline-Si solar cells," *Sci. Rep.*, Vol. 6, 1–11, 2016.
13. Ma, R. M., R. F. Oulton, V. J. Sorger, G. Bartal, and X. A. Zhang, "Room-temperature sub-diffraction-limited plasmon laser by total internal reflection," *Nat. Mater.*, Vol. 10, 110–113, 2011.
14. Azzam, S. I., A. V. Kildishev, R. M. Ma, C. Z. Ning, R. Oulton, V. M. Shalaev, M. I. Stockman, J. L. Xu, and X. Zhang, "Ten years of spasers and plasmonic nanolasers," *Light.: Sci. Appl.*, Vol. 9, 1–21, 2020.
15. Gentile, F., M. L. Coluccio, R. P. Zaccaria, M. Francardi, G. Cojoc, G. Perozziello, R. Raimondo, P. Candeloro, and E. Di Fabrizio, "Selective on site separation and detection of molecules in diluted solutions with super-hydrophobic clusters of plasmonic nanoparticles," *Nanoscale*, Vol. 6, 8208–8225, 2014.
16. Yang, A. K., M. D. Huntington, M. F. Cardinal, S. S. Masango, R. P. van Duyne, and T. W. Odom, "Hetero-oligomer nanoparticle arrays for plasmon-enhanced hydrogen sensing," *ACS Nano*, Vol. 8, 7639–7647, 2014.
17. Chen, J., Q. Zhang, C. Peng, C. Tang, X. Shen, L. Deng, and G. S. Park, "Optical cavity-enhanced localized surface plasmon resonance for high-quality sensing," *IEEE Photon. Technol. Lett.*, Vol. 30, 728–731, 2018.
18. Wu, D., R. Li, Y. Liu, Z. Yu, L. Yu, L. Chen, C. Liu, R. Ma, and H. Ye, "Ultra-narrow band perfect absorber and its application as plasmonic sensor in the visible region," *Nanoscale Research Letters*, Vol. 12, 1–11, 2017.
19. Chen, C., G. Wang, Z. Zhang, and K. Zhang, "Dual narrow-band absorber based on metal-insulator-metal configuration for refractive index sensing," *Opt. Lett.*, Vol. 43, 3630–3633, 2018.
20. Jiang, N., X. Zhuo, and J. Wang, "Active plasmonics: Principles, structures and applications," *Chem. Rev.*, Vol. 118, 3054–3099, 2018.
21. Proietti Zaccaria, R., A. Alabastri, F. De Angelis, G. Das, C. Liberale, A. Toma, A. Giugni, L. Razzari, M. Malerba, H. B. Sun, and E. Di Fabrizio, "Fully analytical description of adiabatic compression in dissipative polaritonic structures," *Phys. Rev. B*, Vol. 86, 035410, 2012.
22. Duan, Q., Y. Liu, S. Chang, H. Chen, and J. Chen, "Surface plasmonic sensors: Sensing mechanism and recent applications," *Sensors*, Vol. 21, 5262, 2021.
23. Špačková, B., P. Wrobel, M. Bocková, and J. Homola, "Optical biosensors based on plasmonic nanostructures: A review," *Proceedings of the IEEE*, Vol. 104, 2380–2408, 2016.

24. Kasani, S., K. Curtin, and N. Wu, "A review of 2D and 3D plasmonic nanostructure array patterns: Fabrication, light management and sensing applications," *Nanophotonics*, Vol. 8, 2065–2089, 2019.
25. Perahia, R., T. P. M. Alegre, A. H. Safavi-Naeini, and O. Painter, "Surface-plasmon mode hybridization in subwavelength microdisk lasers," *Appl. Phys. Lett.*, Vol. 95, 201114, 2009.
26. Cheng, P. J., Z. T. Huang, J. H. Li, B. T. Chou, Y. H. Chou, W. C. Lo, K. P. Chen, T. C. Lu, and T. R. Lin, "High performance plasmonic nanolasers with a nanotrench defect cavity for sensing applications," *ACS Photonics*, Vol. 5, 2638–2644, 2018.
27. Park, S. J., Y. D. Kim, H. W. Lee, H. J. Yang, J. Y. Cho, Y. K. Kim, and H. Lee, "Enhancement of light extraction efficiency of OLEDs using Si_3N_4 -based optical scattering layer," *Opt. Express*, Vol. 22, 12392–12397, 2014.
28. Amiria, I. S., R. Zakaria, and P. Yupapin, "Manipulating of nanometer spacing dual-wavelength by controlling the apodized grating depth in microring resonators," *Results in Physics*, Vol. 12, 32–37, 2019.
29. Johnson, P. B. and R. W. Christy, "Optical constants of the noble metals," *Phys. Rev. B*, Vol. 6, 4370–4379, 1972.
30. Fawzy, S. M., A. M. Mahmoud, Y. I. Ismail, and N. K. Allam, "Novel silicon bipodal cylinders with controlled resonances and their use as beam steering metasurfaces," *Sci. Rep.*, Vol. 11, 13635, 2021.
31. Azzam, S. I., V. M. Shalaev, A. Boltasseva, and A. V. Kildishev, "Formation of bound states in the continuum in hybrid plasmonic-photonic systems," *Phys. Rev. Lett.*, Vol. 121, 253901, 2018.
32. Christ, A., S. G. Tikhodeev, N. A. Gippius, J. Kuhl, and H. Giessen, "Waveguide-plasmon polaritons: Strong coupling of photonic and electronic resonances in a metallic photonic crystal slab," *Phys. Rev. Lett.*, Vol. 91, 183901, 2003.
33. Wang, H., H. Y. Wang, A. Bozzola, A. Toma, S. Panaro, W. Raja, A. Alabastri, L. Wang, Q. D. Chen, H. L. Xu, F. De Angelis, H. B. Sun, and R. P. Zaccaria, "Dynamics of strong coupling between J-aggregates and surface plasmon polaritons in subwavelength hole arrays," *Adv. Funct. Mat.*, Vol. 26, 6198–6205, 2016.
34. Wang, H., A. Toma, H. Y. Wang, A. Bozzola, E. Miele, A. Haddadpour, G. Veronis, F. De Angelis, L. Wang, Q. D. Chen, H. L. Xu, H. B. Sun, and R. P. Zaccaria, "The role of Rabi splitting tuning in the dynamics of strongly coupled J-aggregates and surface plasmon polaritons in nanohole arrays," *Nanoscale*, Vol. 8, 13445–13453, 2016.
35. Abutoama, M. and I. Abdulhalim, "Angular and intensity modes self-referenced refractive index sensor based on thin dielectric grating combined with thin metal film," *IEEE J. Sel. Topics Quantum Electron.*, Vol. 23, 4600309, 2017.
36. Zhou, Y., X. Li, S. Li, Z. Guo, P. Zeng, J. He, D. Wang, R. Zhang, M. Lu, S. Zhang, and X. Wu, "Symmetric guided-mode resonance sensors in aqueous media with ultrahigh figure of merit," *Opt. Express*, Vol. 27, 34788–34802, 2019.
37. Zhu, S. Y., H. L. Li, M. S. Yang, and S. W. Pang, "Highly sensitive detection of exosomes by 3D plasmonic photonic crystal biosensor," *Nanoscale*, Vol. 10, 19927–19936, 2018.
38. Nair, S., C. Escobedo, and R. G. Sabat, "Crossed surface relief gratings as nanoplasmonic biosensors," *ACS Sensors*, Vol. 2, 379–385, 2017.
39. Chen, J., Q. Zhang, C. Peng, C. Tang, X. Shen, L. Deng, and G.-S. Park, "Optical cavity-enhanced localized surface plasmon resonance for high-quality sensing," *IEEE Photon. Technol. Lett.*, Vol. 30, 728–731, 2018.
40. Gong, Y. K., S. Wong, A. J. Bennett, D. L. Huffaker, and S. S. Oh, "Topological insulator laser using valley-hall photonic crystals," *ACS Photonics*, Vol. 7, 2089–2097, 2020.
41. Liu, N., H. Wei, J. Li, Z. Wang, X. Tian, A. Pan, and H. Xu, "Plasmonic amplification with ultra-high optical gain at room temperature," *Sci. Rep.*, Vol. 3, 1967, 2013.
42. Visser, T. D., H. Blok, and B. Demeulenaere, "Confinement factors and gain in optical amplifiers," *IEEE J. Sel. Topics Quantum Electron.*, Vol. 33, 1763–1766, 1997.

43. Yang, A., T. B. Hoang, M. Dridi, C. Deeb, M. H. Mikkelsen, G. C. Schatz, and T. W. Odom, "Real-time tunable lasing from plasmonic nanocavity arrays," *Nat. Commun.*, Vol. 6, 6936, 2015.
44. Verma, R. and B. D. Gupta, "A novel approach for simultaneous sensing of urea and glucose by spr based optical fiber multianalyte sensor," *Analyst.*, Vol. 139, 1449–1455, 2014.
45. Ge, C., M. Lu, S. George, T. A. Flood, C. Wagner, J. Zheng, A. Pokhriyal, J. G. Eden, P. J. Hergenrother, and B. T. Cunningham, "External cavity laser biosensor," *Lab Chip*, Vol. 13, 1247–1256, 2013.
46. Xu, Y., P. Bai, X. Zhou, Y. Akimov, C. E. Png, L. K. Ang, W. Knoll, and L. Wu, "Optical refractive index sensors with plasmonic and photonic structures: Promising and inconvenient truth," *Adv. Opt. Mater.*, Vol. 7, 1801422, 2019.
47. Elshorbagy, M. H., A. Cuadrado, G. González, F. J. González, and J. Alda, "Performance improvement of refractometric sensors through hybrid plasmonic-Fano resonances," *J. Lightwave Technol.*, Vol. 37, 2905–2913, 2019.
48. Zhang, M., M. Lu, C. Ge, and B. T. Cunningham, "Plasmonic external cavity laser refractometric sensor," *Opt. Express*, Vol. 22, 20347–20357, 2014.
49. Shen, Y., J. Zhou, T. Liu, Y. Tao, R. Jiang, M. Liu, G. Xiao, J. Zhu, Z. K. Zhou, X. Wang, C. Jin, and J. Wang, "Plasmonic gold mushroom arrays with refractive index sensing figures of merit approaching the theoretical limit," *Nat. Commun.*, Vol. 4, 2381, 2013.